

Enhancement in magnetic anisotropy in $Co_{40}Fe_{40}B_{20}$ /Fullerene bilayers

Purbasha Sharangi¹, Esita Pandey¹, Shaktiranjan Mohanty¹, Sagarika Nayak¹, Subhankar Bedanta^{1,2}

¹ Laboratory for Nanomagnetism and Magnetic Materials (LNMM), School of Physical Sciences, National Institute of Science Education and Research (NISER), HBNI, P.O.- Bhimpur Padanpur, Via Jatni, 752050, India

² Center for Interdisciplinary Sciences (CIS), National Institute of Science Education and Research (NISER), HBNI, Jatni, 752050 India

E-mail: sbedanta@niser.ac.in

April 2021

Abstract. Organic semiconductor/ferromagnetic bilayer thin films can exhibit novel properties due to the formation of the spinterface at the interface. Buckminsterfullerene (C_{60}) has been shown to exhibit ferromagnetism at the interface when it is placed next to a ferromagnet (FM) such as Fe or Co. Formation of spinterface occurs due to the orbital hybridization and spin polarised charge transfer at the interface. In this work, we have demonstrated that one can tune the magnetic anisotropy of the low Gilbert damping alloy CoFeB by introducing a C_{60} layer. We have shown that anisotropy is enhanced by increasing the thickness of C_{60} which might be a result of the formation of spinterface. However, the magnetic domain structure remains same in the bilayer samples as compared to the reference CoFeB film.

Keywords: Fullerene, Spinterface, Magnetic anisotropy, Domain, Ferromagnetic resonance.

1. Introduction:

Organic spintronics has drawn immense research interest in the last few decades due to its applications in spin valve, magnetic tunnel junctions etc [1, 2, 3]. In organic spintronics, organic semiconductors (OSCs) (e.g. C_{60} , Alq_3 , rubrene etc.) are used to transport or control spin polarized signals [4, 5, 6, 7, 8]. The main advantage of OSCs are their low production cost, light weight, flexible and chemically interactive nature. Usually the spin orbit coupling is small in organic materials (e.g. C_{60}) as they consist of low Z (atomic number) materials (in particular carbon (C)). Moreover, the zero hyperfine interaction in C_{60} results in a longer spin relaxation time [9, 10, 11, 12, 13, 14, 15]. As a consequence, spin of a carrier weakly interacts in organic environment and spin information is maintained for a long time. There are several reports on organic spin valves, organic light emitting diodes (OLED) using C_{60} as a spacer layer [9, 10, 11, 12, 13, 14, 15, 16]. It has been shown that C_{60} (~ 2 nm) can be magnetized when it is placed next to a ferromagnetic (FM) layer [9, 17, 18, 19]. $d - p$ hybridization at the interface of FM/ C_{60} modifies the density of states (DOS) and exhibits room temperature ferromagnetism. Such kind of interface is known as spinterface [20]. It has been shown that the fundamental magnetic properties like magnetic moment, domain structure and magnetic anisotropy can be tuned by depositing C_{60} on top of a Fe, Co or Fe_4N layer [17, 18, 19, 21]. Using first-principles calculations Han *et al.*, have shown that magnetic anisotropy energy (MAE) of Fe_4N system is changed from out-of-plane to in-plane after inserting a C_{60} layer [21]. Their study indicates a strong $d - p$ hybridization between Fe and C atoms which modifies the MAE of the system [21]. It has been found that ~ 2 nm of C_{60} exhibits magnetic moment $\sim 3\mu_B$ /cage at the Fe/ C_{60} interface [17]. However, to the best of our knowledge no such basic study has been performed on CoFeB system. For spintronic application a low damping material is always desired as it directly affects the speed of a device. The main advantage of taking CoFeB as a ferromagnet is that it exhibits low Gilbert damping parameter and it is amorphous in nature [22]. It is very important to explore the effect of interface of such a system (CoFeB/OSC) to enrich our fundamental knowledge of spinterface.

In this regard, we have prepared a CoFeB/ C_{60} bilayer films and compared the magnetic properties to its reference CoFeB film. Also, we have varied the thickness of C_{60} layer to qualitatively define the extent of spinterface and study any changes in the basic magnetic properties. To study the qualitative nature of the interface, we have performed Kerr microscopy and ferromagnetic resonance (FMR) measurements.

2. Experimental details:

CoFeB reference film with 5.5 nm thickness and bilayer (CoFeB/ C_{60}) samples have been deposited on Si (100) substrate in a multi-deposition high vacuum chamber manufactured by Mantis Deposition Ltd., UK. In the bilayer samples the thickness of CoFeB is fixed to 5.5 nm and the thickness of C_{60} has been varied between 1.1 to 15 nm. The composition of CoFeB considered here is 40:40:20. The base pressure in the chamber was 5×10^{-8} mbar. CoFeB, C_{60} and MgO layers have been deposited using DC sputtering, thermal evaporation and e-beam evaporation techniques, respectively. The samples are named as S1, S2, S3, S4 for thickness of C_{60} ($t_{C_{60}}$) taken as 0, 1.1, 5, 15 nm, respectively. The schematic of the sample structure is shown in figure 1(a) (thicknesses not to be scaled). All the layers were deposited without breaking the vacuum to avoid oxidation and surface contamination. The deposition pressure was 5×10^{-3} mbar for CoFeB and 1×10^{-7} mbar for C_{60} and MgO evaporation. The deposition rate for CoFeB and C_{60} layers were 0.1 and $\sim 0.1 - 0.15$ Å/s, respectively. 2 nm of MgO has been deposited as a capping layer. C_{60} layer has been deposited normal to the substrate whereas CoFeB plume was at 30° w.r.t to the substrate normal due to chamber's in-built geometry.

To understand the growth of each layer and interfaces, cross-sectional TEM has been performed on sample S3 using a high-resolution transmission electron microscope (HRTEM) (JEOL F200, operating at 200 kV and equipped with a GATAN oneview CMOS camera). For the compositional analysis we have performed scanning transmission electron microscopy - energy dispersive x-ray spectroscopy (STEM - EDX). Selected area electron diffraction (SAED) has been performed on sample S3 to investigate the growth of the CoFeB and C_{60} layers (supplementary information figure S1). X-ray reflectivity (XRR) has been performed on all the samples to know the exact thickness and roughness of all the layers (supplementary information figure S2 and table R1).

We have measured the hysteresis loop and magnetic domain images at room temperature by magneto-optic Kerr effect (MOKE) based microscopy manufactured by Evico magnetics GmbH, Germany. Longitudinal hysteresis loops are recorded for ± 5 mT magnetic field by varying the angle (ϕ) between the easy axis (EA) and the applied magnetic field direction.

In order to determine the magnetic anisotropy constant and observe the anisotropy symmetry in the samples, angle dependent FMR measurements have been performed at a frequency of 7 GHz for each 5° interval. During the measurement the sample was kept on the wide coplanar waveguide (CPW) in a flip-chip manner. Frequency dependent FMR measurements

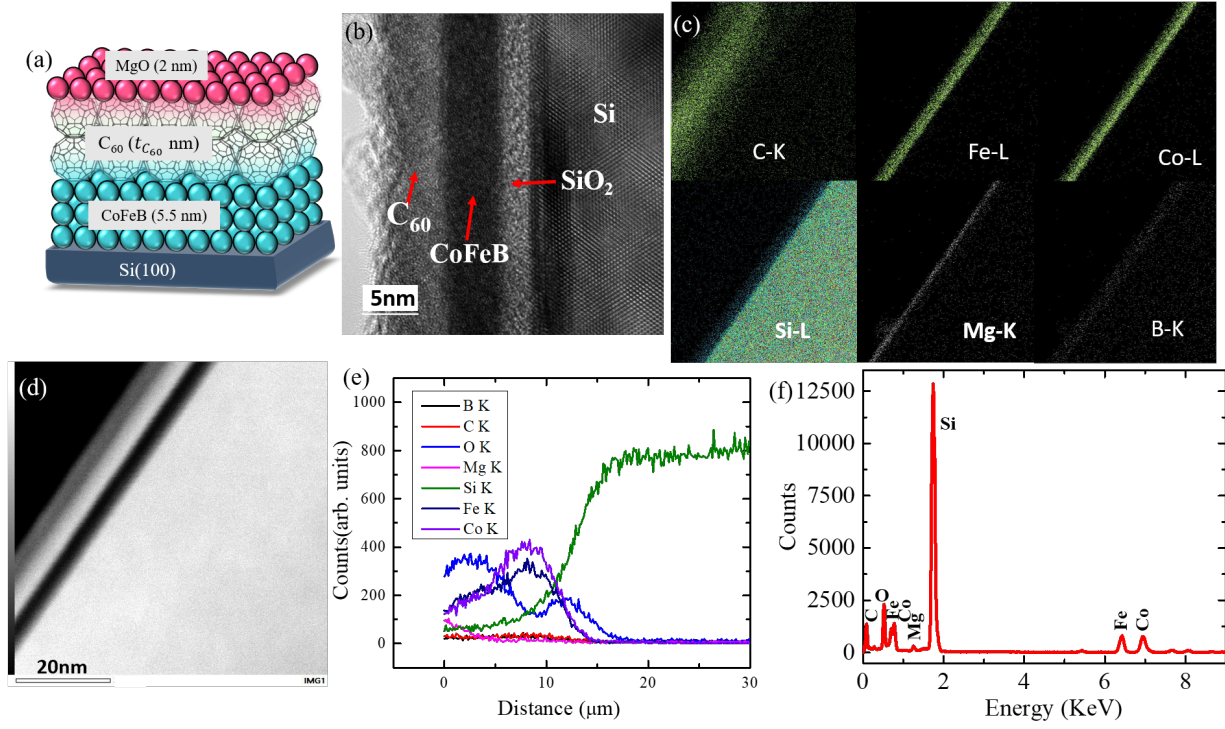


Figure 1. (a) Schematic of the sample structure where, $t_{C_{60}} = 0, 1.1, 5, 15$ nm for samples S1, S2, S3 and S4, respectively. The thicknesses shown in this schematic is not to be scaled to the thicknesses of the samples. (b) Cross-sectional transmission electron microscopy (TEM) image of S3. (c) Elemental mapping for individual layers. (d) The region of the sample S3 where the STEM-EDX has been performed. (e) EDX line profile for each layer of the sample S3. (f) EDX spectrum of sample S3 showing the presence of different elements.

have been performed to calculate the Gilbert damping constant (α).

3. Results and discussion:

High resolution TEM image is shown in figure 1(b) and all the layers are marked separately. It shows the amorphous growth of CoFeB and C_{60} (see supplementary information figure S1). Element specific mapping has been shown in figure 1(c). Figure 1(d) shows the STEM image where, the brighter part indicates the layer of the element having high atomic number (Z). Presence of Boron (B) is not properly visible as it is a lighter atom. Figure 1(e) and (f) represent the EDX line profile and EDX spectra, respectively. The position of the Co and Fe peak at the same place indicates the formation of CoFeB alloy. EDX spectra shows the presence of C, Mg, O, Fe and Co elements in the sample.

Figure 2 shows the in-plane angle (ϕ) dependent hysteresis loops measured using longitudinal magneto optic Kerr effect (LMOKE) microscopy at room temperature for the samples (a) S1, (b) S2 and (c) S3. ϕ is defined as the angle between the EA and the applied magnetic field direction. Angle dependent hysteresis loops show that the magnetic hard axis (HA)

of the samples is at 90° w.r.t the EA, which marks the presence of uniaxial anisotropy in the system. Due to the oblique angle deposition of CoFeB magnetic layer we have observed uniaxial anisotropy in all the samples [19, 23, 24, 25, 26]. It should be noticed that there is a change in coercive field (H_C) in the bilayer samples as compared to the single layer reference sample. The values of H_C are 1.23, 0.70 and 1.55 mT for the samples S1, S2 and S3, respectively. Change in H_C can be attributed to the formation of a spinterface between the CoFeB and C_{60} interface. In our previous study we have shown that the orbital hybridization at the FM (Fe or Co)/ C_{60} interface promote the change in anisotropy of the system [17, 18, 19].

The square shaped loop along EA indicates the magnetization reversal via domain wall motion whereas, along HA the reversal occurs via coherent rotation. The magnetization reversal is studied as a function of ϕ . By varying the angle (ϕ) w.r.t easy axis (0°), we have recorded the domain images near the H_C at $\phi = 0^\circ, 30^\circ, 45^\circ, 60^\circ$ and 90° . Figure 3(a)-(e), (f)-(j) and (k)-(o) shows the magnetic domain images near H_C for the samples S1, S2 and S3, respectively. Branched domains have been observed in all the samples due to the amorphous growth of CoFeB. Domain images captured at different applied magnetic

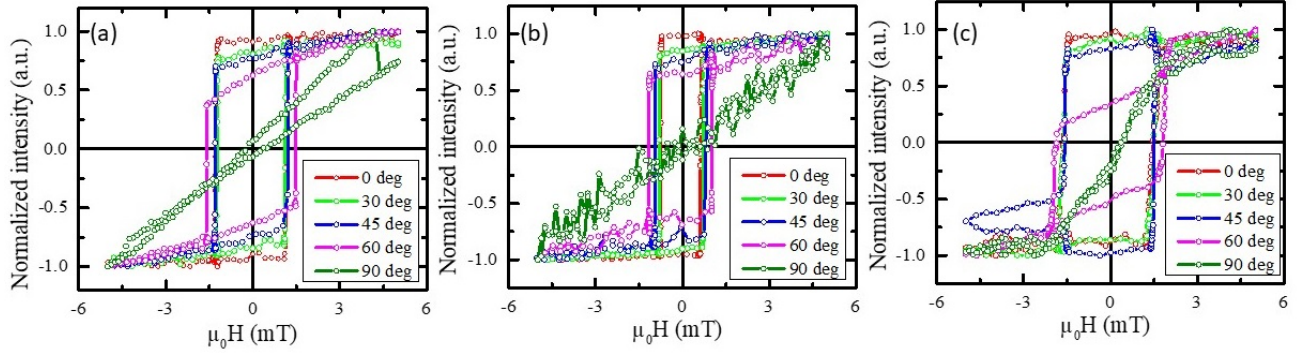


Figure 2. Hysteresis loops measured by magneto optic Kerr effect (MOKE) microscopy at room temperature in longitudinal mode by varying the angle (ϕ) between the easy axis and the applied magnetic field direction for the samples (a) S1, (b) S2 and (c) S3.

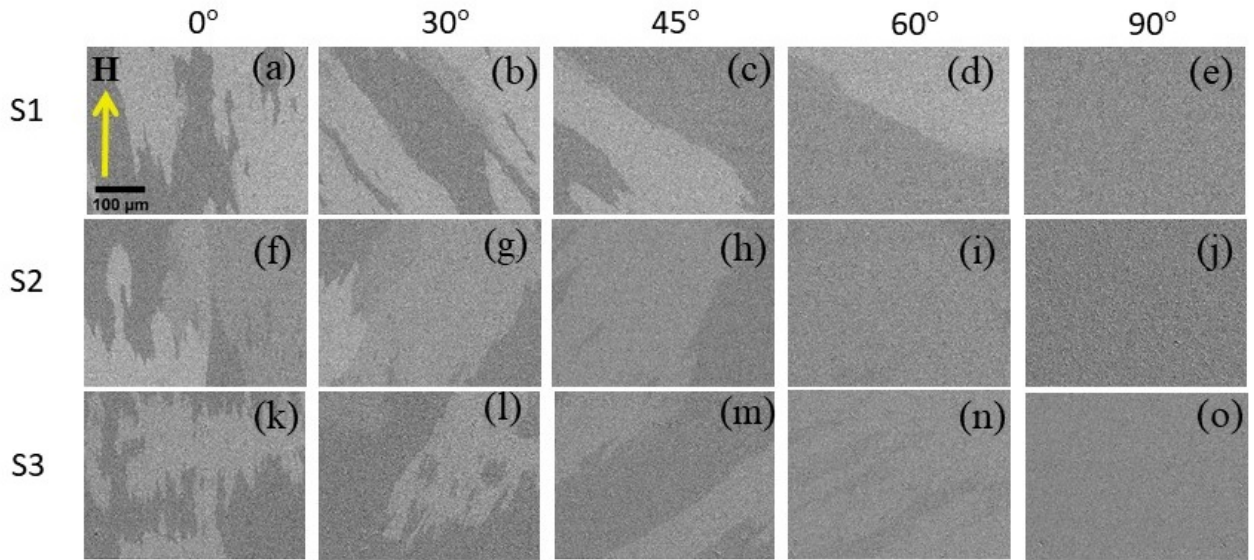


Figure 3. Domain images near H_C for samples S1, S2 and S3 are shown in (a) - (e), (f) - (j) and (k) - (o), respectively. The scale bars of the domain images for all the samples are same and shown in image (a). The applied field (H) direction shown in image (a) was kept constant for all the measurements and the sample was only rotated to capture the domain images at different ϕ .

fields along EA for samples S1, S2 and S3 are shown in figure S3 in supplementary information. Although the H_C is different in all the samples but the change in domain structures is not significant between the single layer CoFeB and the bilayer CoFeB/C₆₀ samples.

We have further investigated the magnetization dynamics by performing the frequency dependent FMR measurement. The experimental data has been fitted using a Lorentzian function (Eq. 1), where ΔH , H_{res} , A_1 and A_2 are linewidth, resonance field, anti-symmetric and symmetric component, respectively [27].

$$FMR_{signal} = A_1 \frac{4\Delta H(H - H_{res})}{(4(H - H_{res}))^2 + (\Delta H)^2} - A_2 \frac{(\Delta H)^2 - 4(H - H_{res})^2}{(4(H - H_{res}))^2 + (\Delta H)^2} + offset \quad (1)$$

The plots of f vs H_{res} and ΔH vs f are shown in figure 4(a) and (b), respectively. The effective damping constant (α) has been determined by fitting the equation 2 and 3 [27, 28, 29]:

$$f = \frac{\gamma}{2\pi} \sqrt{(H_K + H_{res})(H_K + H_{res} + 4\pi M_{eff})} \quad (2)$$

where, γ (gyromagnetic ratio) = $g\mu_B/\hbar$ and g , μ_B , \hbar , H_K are Lande-g factor, Bohr magneton, reduced Planck's constant and anisotropy field, respectively.

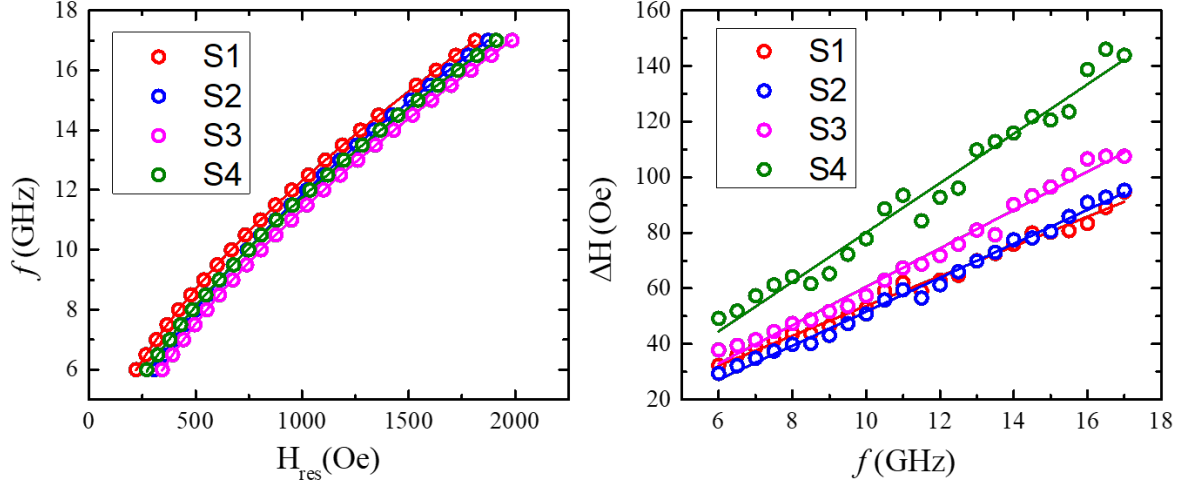


Figure 4. f vs H_{res} and ΔH vs f plots for S1, S2, S3 and S4 are shown in (a) and (b), respectively. Open circles represent the experimental data, while the solid lines are the best fits to the Eq. 2 and 3.

$$\Delta H = \Delta H_0 + \frac{4\pi\alpha f}{\gamma} \quad (3)$$

where, ΔH_0 is the inhomogeneous line width broadening which depends on the magnetic homogeneity of the sample. α values for the samples S1, S2, S3 and S4 are 0.0095 ± 0.0002 , 0.0106 ± 0.0002 , 0.0124 ± 0.0003 and 0.0169 ± 0.0006 , respectively. Change in α might be due to the interface roughness or other effects at the interface. It has been observed that α increases with higher C_{60} thickness.

Table 1. The value of K_2 for all the samples extracted from the fitting of LLG equation.

Sample	K_2 (erg/cc)
S1	2.4×10^4
S2	2.9×10^4
S3	4.1×10^4
S4	4.3×10^4

samples we have performed in-plane angle dependent FMR measurements at a fixed frequency of 7 GHz. Resonance field (H_{res}) has been measured by rotating the sample w.r.t the applied magnetic field in 5° intervals.

H_{res} vs ϕ plots have been shown in figure 5 to calculate the anisotropy constants of the system. The open circles represent the raw data and the solid lines are the best fits. The experimental data is fitted using the Landau-Lifshitz-Gilbert (LLG) equation [30]:

$$f = \frac{\gamma}{2\pi} \left((H + \frac{2K_2}{M_S} \cos 2\phi) (H + 4\pi M_S + \frac{2K_2}{M_S} \cos^2 \phi) \right)^{1/2} \quad (4)$$

where, K_2 is the in-plane uniaxial anisotropy constant, ϕ is the in-plane angle between the easy axis w.r.t the applied magnetic field direction and M_S is the saturation magnetization.

The K_2 values extracted from the fitting are listed in table 1. It has been observed that by introducing a C_{60} layer the anisotropy of the system increased. The possible reason behind the enhancement in the magnetic anisotropy is the formation of spin interface at the $CoFeB/C_{60}$ interface. The anisotropy increases from 2.9×10^4 to 4.1×10^4 erg/cc when the C_{60}

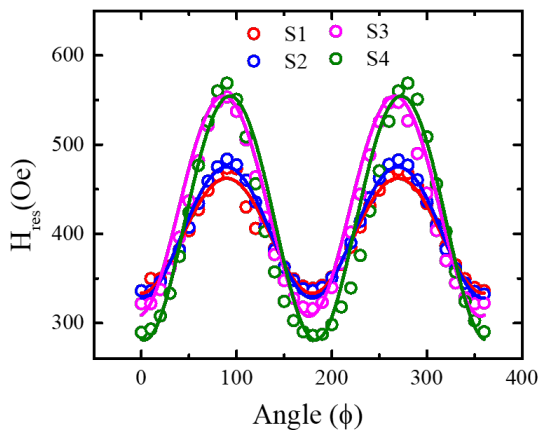


Figure 5. Angle dependent resonance field (H_{res}) plot for all the four samples to calculate the anisotropy constants of the system. The measurement was performed at room temperature at 7 GHz. Open circles represent the experimental data, while the solid lines are the best fits.

To quantify the change in anisotropy in all the

thickness is varied from 1.1 to 5 nm. With further increase in C_{60} thickness (at 15 nm), there is negligible change in the anisotropy (4.1×10^4 to 4.3×10^4 erg/cc). After a certain thickness of C_{60} layer, the spinterface thickness remains almost constant with increasing C_{60} thickness. From our previous study it has been observed that the thickness of the spinterface is ~2 to 3 nm. This clearly states that the anisotropy is more for S3 as compared to S2 with increase in spinterface thickness. Whereas from S3 to S4, increasing the C_{60} thickness does not change the spinterface thickness, thereby keeping the change in anisotropy value negligible.

4. Conclusions:

We have studied the effect of C_{60} on the magnetization reversal and the magnetic anisotropy of a low damping amorphous CoFeB layer. In comparison to the single layer CoFeB sample the magnetic anisotropy constant has increased for the CoFeB/ C_{60} bilayer samples. The anisotropy further increases for the bilayer sample with C_{60} thickness upto 5 nm. However, for bilayer sample with thicker C_{60} layer i.e., 15 nm there is negligible change in anisotropy as compared to the bilayer sample with C_{60} thickness of 5 nm. This behaviour can be understood in terms of the spinterface whose thickness will be in the range of 1 to 3 nm. Further from the Kerr microscopy measurements it is observed that there is negligible change in the branch domain pattern in the samples. The enhancement in the magnetic anisotropy might be the result of $d-p$ hybridization between the CoFeB and C_{60} layer. This study reveals that one can tune the anisotropy of ferromagnetic CoFeB by introducing a C_{60} layer, which can be suitable for the future spintronics devices. Further in future, the nature of spinterface such as thickness, magnetic moment per atom etc. should be investigated by experimental methods such as polarized neutron reflectometry. The results presented here might bring interest to study similar system theoretically to elucidate the exact nature of the spinterface and the origin behind it.

5. Acknowledgments:

We sincerely thank Dr. Tapas Gosh and Mr. Pushpendra Gupta for helping in TEM imaging. The authors also want to thank Dr. Ashutosh Rath for valuable discussion regarding the SAED images. The authors also acknowledge Department of Atomic Energy, and Department of Science and Technology - Science and Engineering Research Board, Govt. of India (DST/EMR/2016/007725) for the financial support.

6. References:

- [1] Naber W, Faez S and van der Wiel W G 2007 *Journal of Physics D: Applied Physics* **40** R205
- [2] Stamps R L, Breitkreutz S, Åkerman J, Chumak A V, Otani Y, Bauer G E, Thiele J U, Bowen M, Majetich S A, Kläui M et al. 2014 *Journal of Physics D: Applied Physics* **47** 333001
- [3] Kuch W and Bernien M 2016 *Journal of Physics: Condensed Matter* **29** 023001
- [4] Dediu V A, Hueso L E, Bergenti I and Taliani C 2009 *Nature materials* **8** 707–716
- [5] Atodiresei N, Brede J, Lazić P, Caciuc V, Hoffmann G, Wiesendanger R and Blügel S 2010 *Physical review letters* **105** 066601
- [6] Barraud C, Seneor P, Mattana R, Fusil S, Bouzehouane K, Deranlot C, Graziosi P, Hueso L, Bergenti I, Dediu V et al. 2010 *Nature Physics* **6** 615–620
- [7] Wang F and Vardeny Z V 2009 *Journal of Materials Chemistry* **19** 1685–1690
- [8] Sun M and Mi W 2018 *Journal of Materials Chemistry C* **6** 6619–6636
- [9] Moorsom T, Wheeler M, Khan T M, Al Ma'Mari F, Kinane C, Langridge S, Bedoya-Pinto A, Hueso L, Teobaldi G, Lazarov V K et al. 2014 *Physical Review B* **90** 125311
- [10] Tran T L A, Wong P K J, de Jong M P, van der Wiel W G, Zhan Y and Fahlman M 2011 *Applied physics letters* **98** 222505
- [11] Tran T L A, C+akir D, Wong P J, Preobrajenski A B, Brocks G, van der Wiel W G and de Jong M P 2013 *ACS applied materials & interfaces* **5** 837–841
- [12] Djeghloul F, Gruber M, Urbain E, Xenioti D, Joly L, Boukari S, Arabski J, Bulou H, Scheurer F, Bertran F et al. 2016 *The journal of physical chemistry letters* **7** 2310–2315
- [13] Gobbi M, Golmar F, Llopis R, Casanova F and Hueso L E 2011 *Advanced Materials* **23** 1609–1613
- [14] Zhang X, Mizukami S, Kubota T, Ma Q, Oogane M, Naganuma H, Ando Y and Miyazaki T 2013 *Nature communications* **4** 1–7
- [15] Nguyen T D, Wang F, Li X G, Ehrenfreund E and Vardeny Z V 2013 *Physical Review B* **87** 075205
- [16] Liu H, Wang J, Groesbeck M, Pan X, Zhang C and Vardeny Z V 2018 *Journal of Materials Chemistry C* **6** 3621–3627
- [17] Mallik S, Mattauch S, Dalai M K, Brückel T and Bedanta S 2018 *Scientific reports* **8** 1–9
- [18] Mallik S, Mohd A S, Koutsoubas A, Mattauch S, Satpati B, Brückel T and Bedanta S 2019 *Nanotechnology* **30** 435705
- [19] Mallik S, Sharangi P, Sahoo B, Mattauch S, Brückel T and Bedanta S 2019 *Applied physics letters* **115** 242405
- [20] Sanvitto S 2010 *Nature Physics* **6** 562
- [21] Han X, Mi W and Wang X 2019 *Journal of Materials Chemistry C* **7** 8325–8334
- [22] Singh B B, Jena S K, Samanta M, Biswas K, Satpati B and Bedanta S 2019 *physica status solidi (RRL)-Rapid Research Letters* **13** 1800492
- [23] Mallik S, Chowdhury N and Bedanta S Aip adv. 4, 097118 (2014)
- [24] Mallik S, Mallick S and Bedanta S 2017 *Journal of Magnetism and Magnetic Materials* **428** 50–58
- [25] Mallik S and Bedanta S 2018 *Journal of Magnetism and Magnetic Materials* **446** 270–275
- [26] Mallick S, Mallik S, Singh B B, Chowdhury N, Gieniusz R, Maziewski A and Bedanta S 2018 *Journal of Physics D: Applied Physics* **51** 275003
- [27] Singh B B, Jena S K and Bedanta S 2017 *Journal of Physics D: Applied Physics* **50** 345001
- [28] Kittel C 1948 *Physical review* **73** 155
- [29] Heinrich B, Cochran J and Hasegawa R 1985 *Journal of*

Applied Physics **57** 3690–3692

[30] Pan S, Seki T, Takanashi K and Barman A 2017 *Physical Review Applied* **7** 064012

Supplementary Information

Enhancement in magnetic anisotropy in $Co_{40}Fe_{40}B_{20}$ /Fullerene bilayers

Purbasha Sharangi^a, Esita Pandey^a, Shaktiranjan Mohanty^a, Sagarika Nayak^a, and Subhankar Bedanta^{*a,b}

^a *Laboratory for Nanomagnetism and Magnetic Materials (LNMM), School of Physical Sciences, National Institute of Science Education and Research (NISER), HBNI, P.O.- Bhimpur Padanpur, Via-Jatni, 752050, India. E-mail: sbedanta@niser.ac.in*

^b *Center for Interdisciplinary Sciences (CIS), National Institute of Science Education and Research (NISER), HBNI, Jatni, 752050 India*

Structural information:

In order to investigate the growth of deposited layers we have performed selected area electron diffraction (SAED) on sample S3 (i.e., CoFeB(5.5nm)/C₆₀ (5 nm)/MgO(2nm)). The SAED image (figure S1) shows the diffuse rings, which confirms the amorphous growth of CoFeB and C₆₀ layers. Further, to know the structural information (thickness, roughness), we have performed X-ray reflectivity (XRR) measurements on all the samples. We have fitted the data by using GenX software. Figure S2 (a), (b), (c) and (d) show the XRR data and best fits for samples S1, S2, S3 and S4, respectively. The extracted thickness and roughness of the layers are shown in Table S1.

Hysteresis loop and domain imaging:

Figure S3 (a), (b) and (c) show the hysteresis loop for the samples S1, S2 and S3, respectively along the easy axis (EA). The domain images are shown in (d) to (r) and also marked in the hysteresis

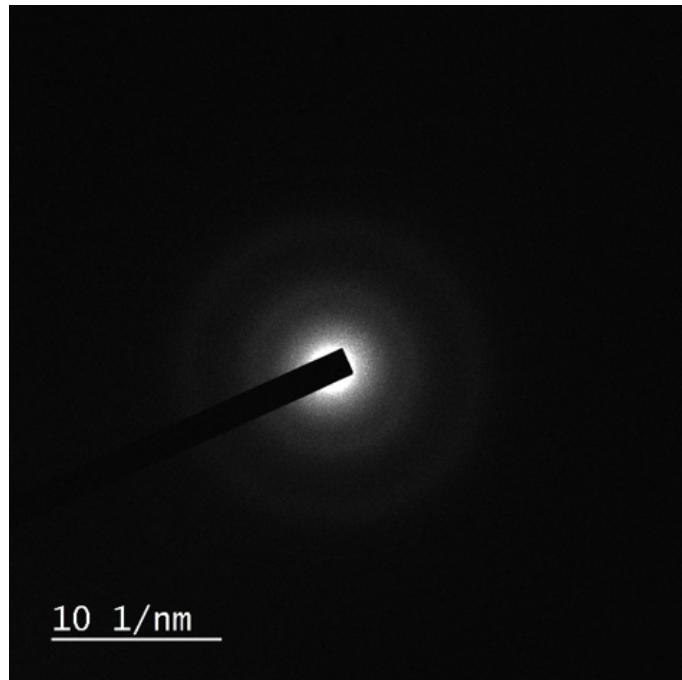


FIG. S1. SAED image of sample S3.

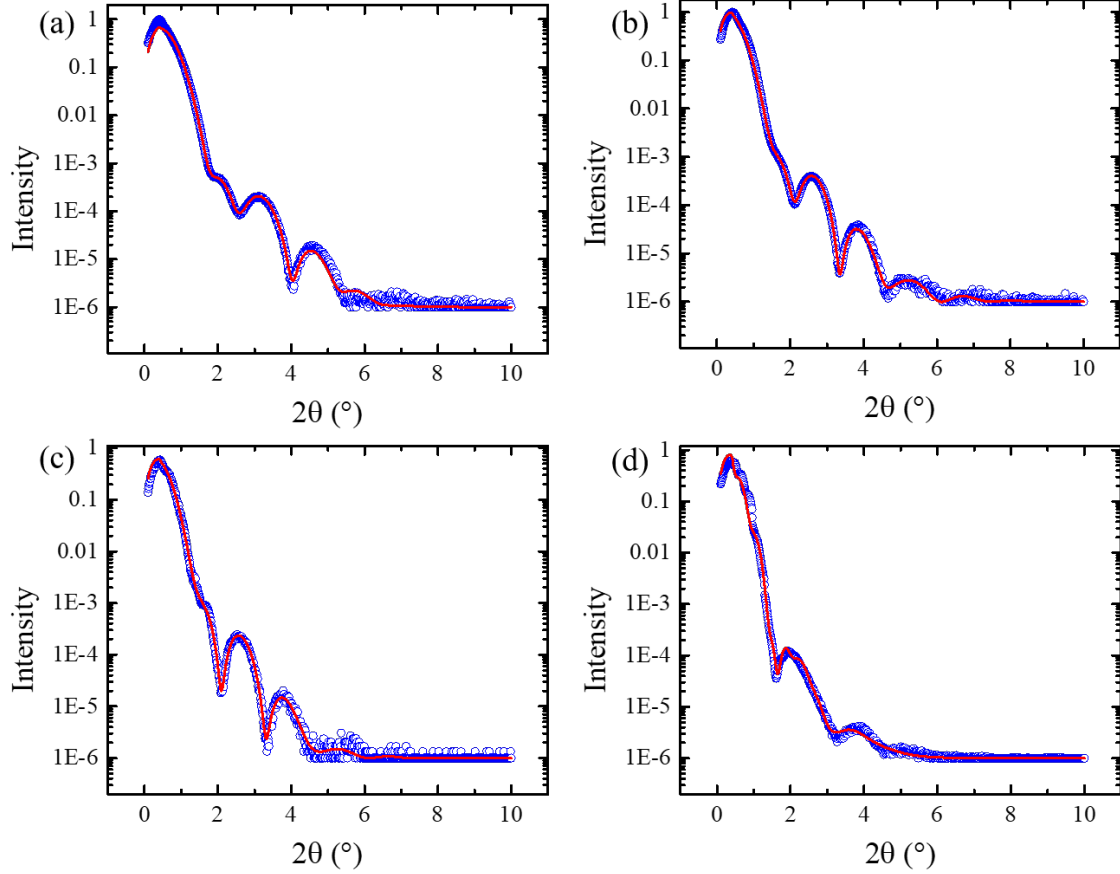


FIG. S2. XRR data and the best fits for samples S1, S2, S3 and S4 are shown in (a), (b), (c) and (d), respectively. The blue open circles are experimental data and the red solid lines represent the best fit using GenX software. The parameters extracted from the best fits are shown in Table S1.

TABLE I. Parameters obtained from XRR fits

Layers	Sample S1		Sample S2		Sample S3		Sample S4	
	Thickness(nm)	Roughness(nm)	Thickness(nm)	Roughness(nm)	Thickness(nm)	Roughness(nm)	Thickness(nm)	Roughness(nm)
CoFeB	5.50	0.91	5.60	0.93	5.80	0.81	5.45	0.96
C ₆₀	-	-	1.10	0.20	5.00	0.52	15.00	1.80
MgO	1.95	0.61	1.90	0.57	2.09	0.76	1.98	0.75

loops. Figure S3 (d), (i) and (n) represent the domain images for S1, S2, S3 captured at positive saturation field. Similarly, (e), (j), (o) are the domain images near nucleation. (f), (k), (p) show the domain images which are captured near coercive field and (g), (l), (q) are captured near negative saturation for samples S1, S2 and S3, respectively. Further, domain images captured at negative saturation field are shown in (h), (m), (r) for S1, S2, and S3, respectively.

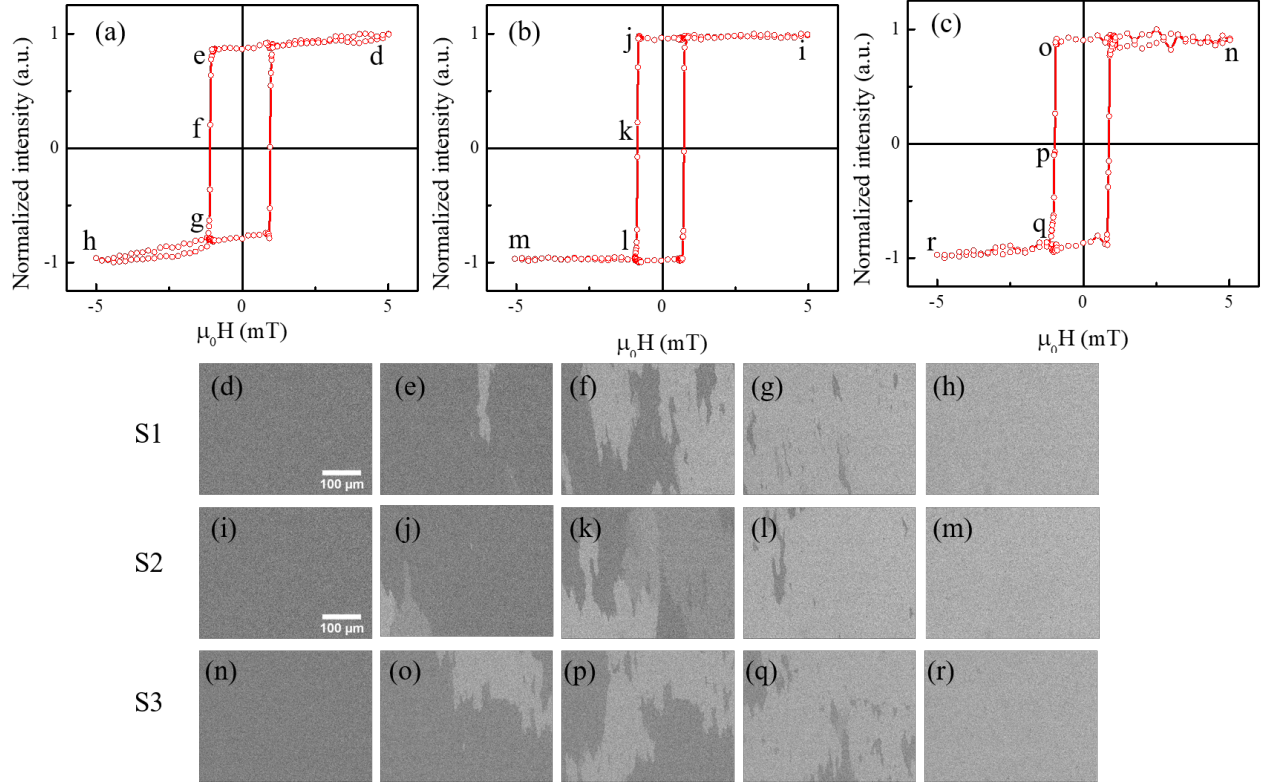


FIG. S3. (a), (b) and (c) show the hysteresis loops for the samples S1, S2 and S3, respectively along the easy axis (EA). The domain images at different applied fields (marked b to r in hysteresis loops) for samples S1, S2 and S3 are shown in figure S3 (d-h), (i-m) and (n-r), respectively.